HHS Public Access

Author manuscript

J Bone Miner Res. Author manuscript; available in PMC 2022 December 01.

Published in final edited form as:

J Bone Miner Res. 2021 December ; 36(12): 2317–2328. doi:10.1002/jbmr.4443.

Conductive hearing loss in the Hyp mouse model of X-linked hypophosphatemia is accompanied by hypomineralization of the auditory ossicles

Maximilian M. Delsmann[1,2,*], **Richard Seist**[3,*], **Julian Stürznickel**[1,2], **Felix N. Schmidt**[1], **Amer Mansour**[3], **Margaret M. Kobelski**[4], **Gabriel Broocks**[5], **Jonathan Peichl**[6], **Ralf Oheim**[1], **Mark Praetorius**[6], **Thorsten Schinke**[1], **Michael Amling**[1], **Marie B. Demay**[4], **Konstantina M. Stankovic**[3,7,8,*], **Tim Rolvien**[2,*]

[1]Department of Osteology and Biomechanics, University Medical Center Hamburg Eppendorf; Hamburg, Germany

[2]Department of Trauma and Orthopaedic Surgery, Division of Orthopaedics, University Medical Center Hamburg-Eppendorf; Hamburg, Germany

[3]Department of Otolaryngology-Head and Neck Surgery, Massachusetts Eye and Ear and Harvard Medical School; Boston, MA, United States

[4]Endocrine Unit, Massachusetts General Hospital, Harvard Medical School; Boston, MA, United States

[5]Department of Diagnostic and Interventional Neuroradiology, University Medical Center Hamburg Eppendorf; Hamburg, Germany.

[6]Department of Otorhinolaryngology, University Medical Center Hamburg-Eppendorf; Hamburg, Germany

[7]Program in Speech and Hearing Bioscience and Technology, Harvard Medical School; Boston, MA, USA

[8]Harvard Program in Therapeutic Science, Harvard University; Boston, MA, USA

Abstract

X-linked hypophosphatemia (XLH) is a hereditary musculoskeletal disorder caused by loss-of-function mutations in the *PHEX* gene. In XLH, increased circulating fibroblast growth factor 23 (FGF23) levels cause renal phosphate wasting and low concentrations of 1,25-dihydroxyvitamin D, leading to an early clinical manifestation of rickets. Importantly, hearing loss is commonly observed in XLH patients. We here present data from two XLH patients with marked conductive

Corresponding Authors: Tim Rolvien, MD, PhD, Department of Trauma and Orthopaedic Surgery, University Medical Center Hamburg-Eppendorf, Martinistraße 52, 20246 Hamburg, Germany, Phone: +49-40-7410-52670, t.rolvien@uke.de; Konstantina M. Stankovic, MD, PhD, Department of Otolaryngology Head and Neck Surgery, Massachusetts Eye and Ear, 243 Charles St, Boston, Massachusetts, the USA. Konstantina_stankovic@meei.harvard.edu.

*These authors contributed equally to this work.

Author Contributions: M.M.D., R.S., M.A., M.B.D., K.M.S. and T.R. designed research; M.M.D., R.S., J.S., F.N.S., A.M., M.M.K., J.P., M.P., T.S., and M.B.D. performed research; M.M.D., R.S., J.S., F.N.S., A.M., M.M.K., G.B., R.O., M.P., T.S., M.A., M.B.D., K.M.S. and T.R. analyzed data; and M.M.D., R.S., K.M.S. and T.R. wrote the paper.

Disclosures: All authors state that they have no conflict of interest and nothing to disclose.

hearing loss. To decipher the underlying pathophysiology of hearing loss in XLH, we utilized the *Hyp* mouse model of XLH and measured auditory brain stem responses (ABRs) and distortion product otoacoustic emissions (DPOAEs) to functionally assess hearing. As evidenced by the increased ABR/DPOAE threshold shifts in the mid-frequency range, these measurements indicated a predominantly conductive hearing loss in *Hyp* mice compared to wild type (WT) mice. Therefore, we carried out an in-depth histomorphometric and scanning electron microscopic analysis of the auditory ossicles. Quantitative backscattered electron imaging (qBEI) indicated a severe hypomineralization of the ossicles in *Hyp* mice, evidenced by lower calcium content (CaMean) and higher void volume (i.e., porosity) compared to WT mice. Histologically, voids correlated with unmineralized bone (i.e., osteoid), and the osteoid volume per bone volume (OV/BV) was markedly higher in *Hyp* mice than WT mice. The density of osteocyte lacunae was lower in *Hyp* mice than in WT mice, whereas osteocyte lacunae were enlarged. Taken together, our findings highlight the importance of ossicular mineralization for hearing conduction and point towards the potential benefit of improving mineralization to prevent hearing loss in XLH.

Introduction

X-linked hypophosphatemia (XLH) is a hereditary musculoskeletal disorder caused by a loss-of-function mutation in the *PHEX* gene (phosphate regulating endopeptidase homolog X-linked; located at Xp22.1) affecting approximately 1:20,000 individuals [(1)]. *PHEX* is mainly expressed in osteoblasts and encodes a protein which belongs to the type II cell integral membrane zinc-dependent proteases. How this mutation leads to increases in fibroblast growth factor 23 (FGF23) expression remains unknown [(2,3)]. In XLH, increased levels of the phosphaturic hormone FGF23 result in renal phosphate wasting [(4)]. Additionally, FGF23 causes inhibition of the renal 1α-hydroxylase (CYP27B1) and induces expression of 24-hydroxylase (CYP24A1), resulting in decreased levels of 1,25-dihydroxyvitamin D ($1,25(OH)_2D$) [(5)].

Chronic hypophosphatemia in XLH leads to rickets, characterized by expansion of the hypertrophic chondrocyte layer of the growth plate, accompanied by osteomalacia, due to hypomineralization of the bone [(6–8)] and an increase in osteoid volume [(9,10)]. Impaired skeletal microarchitecture has been detected in both the cortical and trabecular compartment in form of increased cortical porosity and reduced trabecular number, respectively, in both mice and humans [(6,10)]. Clinical manifestation of XLH is usually within the first two years of life with a progressive bowing of the lower limbs (i.e., valgus or varus malalignment) and a disproportionate short body stature [(11,12)]. Dental abnormalities including enamel defects and abscessed non-carious teeth are observed [(12)] as may be cranial abnormalities such as cranial synostosis or Chiari type I malformation [(13)].

Importantly, an increased prevalence of sensorineural and conductive hearing loss in patients with XLH is described, ranging from 16–76% of affected subjects [(14–17)]. Sensorineural and conductive hearing loss occur due to pathologies in the sensory organ (i.e., the cochlea) and the middle ear containing the auditory ossicles, respectively. Due to other confounding factors such as age or environmental factors, the exact mechanisms that contribute to hearing loss in XLH remain elusive. Specifically, while ossicles normally exhibit exceptionally

high matrix mineralization along with low bone remodeling [18,19], it is unknown whether the observed hearing loss in XLH is linked to hypomineralization of auditory ossicles. In order to decipher the mechanisms of hearing loss in XLH, we functionally assessed hearing in the *Hyp* mouse model of XLH utilizing auditory brain stem responses (ABRs) and distortion product otoacoustic emissions (DPOAEs). We complemented functional studies with histological, histomorphometric, and microstructural analyses of the ossicles in *Hyp* compared to WT mice, with focus on the ossicles' mineralization properties. Our results reveal a mechanism of hearing loss in *Hyp* mice and strongly motivate future studies to prevent or reverse this hearing loss.

Materials & Methods

XLH patients

XLH patients carrying verified *PHEX*-mutations presented to our specialized outpatient clinic (the National Bone Board) at the University Medical Center Hamburg-Eppendorf. Hearing tests were performed within the routine clinical workup in collaboration with the Department of Otorhinolaryngology. Cranial computed tomography (CCT) scans were evaluated in the two XLH patients affected by conductive hearing loss to determine the mineralization of the ossicles in XLH and non-XLH patients by quantification of Hounsfield units (HU). For this purpose, the region of interest (ROI), i.e., the region representing the largest cross-section of the ossicles, was determined in axial views. The determined HU reflected the mean value of this area. Control values were obtained from age- and sex-matched anonymized CCT scans performed at our institution in patients with concussion after trauma to exclude intracranial hemorrhage.

The two XLH patients affected by conductive hearing loss had also undergone standardized iliac crest biopsy to determine detailed parameters of bone mineralization. To interpret the obtained histomorphometric data of the iliac crest biopsies, we analyzed four sex- and age-matched control biopsies (all female, 20, 22, 25 and 40 years, mean±SD: 26.8±9.1 years), which had been previously acquired from skeletally-healthy individuals in the context of a previous cadaveric study [20]. Patient data collection and analysis was approved by the local ethics committee (no. PV5364/PV7046). Informed written consent was obtained from all patients. All investigations were carried out in line with the Declaration of Helsinki.

Animals and experimental design

All mice tested were from a C57BL/6 background. For measuring ABR and DPOAE, nine male *Hyp* and six male WT mice at the age of six weeks were analyzed, a time point before the onset of age-related hearing loss [21]. For the high-resolution skeletal analysis of the ossicles in *Hyp* mice, five male *Hyp* mice at the age of 24 weeks were examined and compared with five male WT mice of the same age and background. In the developmental analysis of the ossicles, five age groups (3, 6, 12 and 24 weeks) of wild type (WT) mice were examined. Each group consisted of five mice. All organ preparations from *Hyp* and WT mice have been approved by the "Behörde für Umwelt und Gesundheit der Hansestadt Hamburg" (Org529, G14/68). Animal husbandry and interventions were approved by the

institutional Animal Care and Use Committee of Massachusetts Eye and Ear and conducted in accordance with the NIH Guide for the Care and Use of Laboratory Animals.

Hearing tests

Cochlear function was tested by measuring ABRs and DPOAEs in 9 *Hyp* and 6 WT male mice. Mice were anesthetized with intraperitoneal ketamine (100 mg/kg) and xylazine (10 mg/kg). To provide a clear view and access to the tympanic membrane, a small incision was made in the external ear canal. A custom acoustic system coupled to a probe tube was used consisting of two miniature earphones (CDMG15008–03A, CUI, Tualatin, USA) serving as sound sources and a microphone (FG-23329-P07, Knowles, Itasca, USA) to measure sound pressure near the eardrum. DPOAEs were measured as ear canal pressure in response to two tones presented into the ear canal (f1 and f2, with f2 / f1 = 1.2 and f1 being 10 dB above f2) at half-octave steps from f2 = 5.66 – 45.25 kHz, and in 5 dB intensity increments from 10 to 80 dB SPL. DPOAE thresholds were defined as the f2 intensity required to generate a DP response of 10 dB SPL over noise floor. ABRs to 5 ms tone pips were measured between subdermal electrodes (adjacent to the ipsilateral incision, at the vertex, and near the tail), amplified 10,000 times, and filtered through a 0.3–3.0 kHz bandpass filter. For each frequency, the sound level starting below the threshold was increased in 5 dB-steps and 512 responses were recorded and averaged using custom LabVIEW data-acquisition software run on a PXI chassis (National Instruments Corp., Austin, USA). ABR thresholds were defined as the lowest level at which a repeatable waveform could be visually detected. The ratios of the summating potential (SP) to the auditory nerve action potential (AP), called SP/AP, were analyzed. Of note, an increased SP/AP ratio correlates with endolymphatic hydrops-related diseases such as Menière's disease [22,23].

Micro-computed tomography (μ-CT)

To visualize the anatomical position and phenotype of the ossicles in the temporal bone, the ossicles were imaged using a high-resolution μ-CT System (Skyscan 1272, Bruker, Kontich, Belgium). The scans were conducted at a resolution of 6 μm at 90 kV and 111 μA with a 0.5 mm aluminum filter.

Histology

Transiliac crest biopsies and murine skeletons were prepared for undecalcified histology following a standardized protocol. Mice were sacrificed via CO_2 inhalation and the skeletons were fixed in 3.7% PBS-buffered formaldehyde for 48 h and subsequently stored in 80% ethanol. The preparation and isolation of the ossicles was performed under a stereo microscope. All specimens (transiliac crest biopsies, auditory ossicles) were dehydrated in an ascending ethanol series, embedded undecalcified in methyl-methacrylate, and cut on a rotation microtome (CVT 4060E, microTec, Walldorf, Germany) to generate 4 μm thick sections. The sections were subsequently stained with toluidine blue and von Kossa-van Gieson. Histomorphometric analysis was carried out according to the *ASBMR* guidelines [24], including bone volume to tissue volume (BV/TV, %) and the osteoid volume per bone volume (OV/BV, %).

Additionally, the cochleae were extracted from the temporal bones, flushed carefully with PFA through the round and oval windows, post-fixed in PFA for 2h, and decalcified in 0.12 M ethylenediaminetetraacetic acid (EDTA) for 3 days. Decalcified cochleae were dehydrated in a series of graded ethanol, embedded in paraffin, and cut in 10 μm thick serial sections parallel to the mid-modiolar axis using a Leica RM 2155 microtome and mounted on precoated Superfrost Plus glass slides (Thermo Fisher Scientific, Waltham, USA). Sections were deparaffinized with Histo-Clear (National Diagnostics, Atlanta, USA) and rehydrated in a series of graded ethanol, stained with hematoxylin and eosin, mounted with Permount (Thermo Fisher Scientific, Waltham, USA), and imaged on a Leica (Wetzlar, Germany) bright-field microscope.

*Quantitative backscattered electron imaging (*qBEI*)*

For quantitative backscattered electron imaging (qBEI), the specimens were first polished to a coplanar finish before being carbon coated. qBEI was performed using a scanning electron microscope (LEO 435 VP, LEO Electron Microscopy Ltd.; Cambridge, England) with a backscattered electron detector (Type 202; K.E. Developments Ltd.; Cambridge, UK), operated at 20 kV and 680 pA at a constant working distance. Detailed working methods have been described previously [25–27]. The images were analyzed with ImageJ analysis software (ImageJ 1.42, National Institutes of Health, Bethesda, USA) and a custom MATLAB-based program (TheMathWorks, Inc., Natick, USA), respectively. Grey values, which are proportional to calcium content [28], were used to determine the percentage of voids (porosity, %), mean calcium content (CaMean, wt%), mineralization heterogeneity (CaWidth, wt%), and peak calcium content (CaPeak, wt%). Furthermore, number of the osteocyte lacunae (N.Ot.Lc/B.Ar, 1/mm^2) and mean osteocyte lacunar area (Lc.Ar, μm^2) were determined.

Statistical analysis

GraphPad Prism (version 9.0, GraphPad Software, La Jolla, USA) was used for all statistical analyses. Results are expressed as individual values and as means ± standard deviations (SD). Normality of data distribution was tested using the Shapiro-Wilk test. Analysis of data from two groups was performed with paired two-tailed *t*-test for normally distributed data and Mann-Whitney U-test for non-normally distributed data. Statistical significance in ABR and DPOAE data was determined using ordinary two-way ANOVA with subsequent Sidak's test for multiple comparisons. p values <0.05 were considered significant.

Results

Conductive hearing loss in patients with XLH

Seven genetically confirmed female XLH patients recently presented at our outpatient clinic in whom we performed hearing tests (i.e., audiometry) as part of the routine clinical workup (Suppl. Table 1). Two of seven patients (patient 1: 27 years old; patient 2: 32 years old) showed marked conductive hearing loss. Both patients also suffered from treatment-resistant pain of the lower limbs. Patient 1 had a history of three vertebral fractures and patient 2 of multiple (stress) fractures of the pelvis, fibula, humerus and femur, underlining the substantial clinical burden of both patients. Genetic analysis revealed heterozygous *PHEX*

mutations in both patients (patient 1: c.1862A>C and patient 2: c.2229delG). Pure-tone threshold audiometry confirmed bilateral hearing loss, namely an elevated threshold for air conduction compared to bone conduction, indicating conductive hearing loss (Fig. 1 A).

Audiometry in the other five XLH patients did not confirm substantial conductive hearing loss (Suppl. Fig. 1), although three patients (patients 3–5) reported subjective hearing loss. In patient 3, in the presence of tinnitus after sudden sensorineural hearing loss, a low- and high-frequency hearing loss with a leading sensorineural component was detected. In patient 4, a clinically irrelevant high-frequency hearing loss was measured, whereas patients 5–7 had normal audiograms.

In the two XLH patients affected by conductive hearing loss, average hounsfield units (HU) of the auditory ossicles were derived from CCT scans and compared to three CT scans obtained from age-matched healthy women. Quantification revealed lower HU values for the XLH patients than the controls (Fig. 1 B), suggesting impaired bone mineralization. Likewise, the analysis of the obtained transiliac crest biopsy by quantitative backscattered electron imaging (qBEI) revealed a lower mean calcium content (CaMean) and higher fraction of low mineralized bone areas (CaLow) compared to age-matched female controls (Fig. 1 C). Moreover, histomorphometric analysis of transiliac biopsies indicated an elevated osteoid volume per bone volume (OV/BV) and bone volume to tissue volume (BV/TV) compared to controls, pointing to severe osteomalacia (Fig. 1 D).

Functional assessments of hearing indicate a predominant conductive hearing loss in Hyp mice

We assessed the auditory phenotype of 6-week-old male *Hyp* and WT littermates by ABRs which reflects the summed electrical signal of the auditory nerve and central auditory pathways, and DPOAEs which reflect outer hair cell function. ABR thresholds (Fig. 2 A) were increased in *Hyp* mice relative to WT mice, at all measured frequencies except 8 kHz. At 32 kHz, the mean difference of 12.5 dB SPL was statistically significant between the genotypes ($p=0.0169$) by 2-way ANOVA and subsequent Sidak's test for multiple comparisons. DPOAE thresholds (Fig. 2 B) in *Hyp* mice were increased at all measured frequencies relative to WT mice and showed statistical significance at 16 kHz (mean difference = 16.56 dB SPL, $p=0.0447$). Threshold shifts (Fig. 2 C) between *Hyp* and WT mice were similar for ABRs and DPOAEs, except for the mid-frequency region at 16 and 22.65 kHz where DPOAE shifts were twice as large as ABR shifts, consistent with a conductive hearing loss in *Hyp* mice. Plotting the DPOAE I/O function (Fig. 2 D), we observed a rightward shift in *Hyp* mice relative to WT mice; the growth functions in *Hyp* mice were roughly parallel to those in WT mice across different frequencies. This pattern is consistent with conductive hearing loss [(29)] in *Hyp* mice and supports the findings observed in Fig. 2 C.

The auditory brain stem response wave I (Fig. 2 E) is made up of two components: the summating potential (SP) and action potential (AP). In response to tone stimuli, the SP component is the hair cell's potential generated as they move together with the basilar membrane, whereas the AP component represents the collective firing of the auditory nerve fibers. We calculated the SP/AP ratio at 3 frequencies, 8, 16, and 32 kHz (Fig. 2 F). The

SP/AP ratio was significantly increased in *Hyp* mice at all tested frequencies: 8 kHz (mean difference = 0.33 ± 0.06, p<0.0001), 16 kHz (mean difference = 0.51 ± 0.10, p=0.0002) and 32 kHz (mean difference = 0.12 ± 0.04, p=0.0062). Interestingly, SP/AP ratios at 8 and 16 kHz were increased in every *Hyp* mouse measured compared to WT, showing the high sensitivity of this test.

Severe hypomineralization of the auditory ossicles

A visualization of the murine 24-week-old male WT middle ear with fenestration of the temporal bone using μ-CT-imaging is shown in Fig. 3 A. qBEI of the malleus of *Hyp* mice revealed substantially reduced bone mineralization with large voids (Fig. 3 B), indicating a significantly higher porosity in *Hyp* mice (47.31 ± 7.83 %) compared to WT mice (3.94 ± 1.21 %, p<0.0001; Fig. 3 C). Furthermore, the CaMean was significantly lower (26.22 ± 0.29 % *vs.* 30.20 ± 0.10 %, p<0.0001; Fig. 3 D) and the mineralization was significantly more heterogeneous (6.60 ± 0.19 % *vs.* 4.32 ± 0.14 %, p<0.0001; Fig. 3 E) in *Hyp* mice compared to WT mice, evidenced by shifts in the bone mineral density distribution (BMDD) histograms (Fig. 3 F). Additional analysis of osteocyte characteristics revealed a significantly reduced number of osteocyte lacunae per bone (N.Ot.Lc/B.Ar; 1/mm^2) (1538.0 ± 142.7 /mm^2 *vs.* 2001.0 ± 109.2 /mm^2, p=0.004; Fig. 3 G) in *Hyp* mice, while the mean osteocyte lacunar area (Lc.Ar) was significantly larger (33.25 ± 0.79 μm^2 *vs.* 20.37 ± 0.52 μm^2, p<0.0001; Fig. 3 H).

Similar abnormalities in mineralization and osteocyte lacunar characteristics were observed in the stapes (Fig. 3 I) of *Hyp* mice by qBEI (Fig. 3 J). The CaMean was significantly lower in the stapes of *Hyp* mice (26.52 ± 0.40 % *vs.* 28.90 ± 0.26 %, p<0.0001; Fig. 3 K), while the CaWidth (6.10 ± 0.05 % *vs.* 5.48 ± 0.20 %, p=0.0001; Fig. 3 L) and the Lc.Ar (31.13 ± 3.43 μm^2 *vs.* 19.41 ± 1.20 μm^2, p<0.0001; Fig. 3 M) were significantly increased.

Hyp mice exhibit osteomalacia of the ossicles and mild endolymphatic hydrops

Histological analyses of the malleus in 6-week-old mice (Fig. 4 A) revealed a similar BV/TV in *Hyp* mice (97.17 ± 1.88) and WT mice (97.01 ± 1.67). However, the OV/BV was markedly increased in *Hyp* mice (55.69 ± 5.45) relative to WT mice (0.006 ± 0.01, p=0.0079; Fig. 4 B).

In addition to examining the ossicles, the cochleae were examined histologically after completion of electrophysiological tests (Fig. 4 C). Compared to WT mice, *Hyp* mice had high amounts of osteoid in the otic capsule at already 6 weeks; no osteoid was observed in WT mice (Fig. 4 C). While endolymphatic hydrops (ELH) was not detected in any WT mice, five out of seven *Hyp* mice demonstrated ELH in the basal turn (Fig. 4 D). The observed hydrops was very mild in all cases, grade 1 based on the grading system of Melki et al. [23].

Microstructural and cellular characteristics of the ossicles during postnatal development in WT mice

In order to gain a better understanding of the time course of ossicular mineralization, postnatal development of the malleus was examined in WT mice (Fig. 5 A). Analyses of

porosity (i.e., void volume per total bone volume) (Fig. 5 B) revealed voids in three-week-old WT mice, which mineralized rapidly, with the number and volume of voids decreasing with age (week three: 14.51 ± 1.89 %, week six: 4.68 ± 1.84 %, p=0.0003). After the 6th week of life, no significant changes in porosity were detected. In line with this observation, a significant increase of CaMean from 28.77 ± 0.52 wt % (week three) to 31.48 ± 0.43 wt % (week 24) was detected (p=0.0006; Fig. 5 C). Furthermore, the osteocyte lacunae were reduced in number and area between weeks three and 24 (number week three: 2382.90 ± 177.49 1/mm^2; week 24: 1474.23 ± 95.90 1/mm^2, p=0.0001; Fig. 5 D) (area week three: 18.53 ± 0.86 μm^2, week 24: 15.74 ± 1.05 μm^2, p=0.0263; Fig. 5 E).

Voids on qBEI analysis were found to be contain blood vessels with mesenchymal cells. During the postnatal development, an early regression of the blood vessels was observed (Fig. 5 F); these vessels were replaced by bone matrix formed by osteoblasts. While prominent voids with blood vessels were still visible in 20-day old mice, these luminae were already reduced by week six (Fig. 5 G). In mice at 24 weeks of age (Fig. 5 H), only small persistent blood vessels with few erythrocytes or small areas of osteoid were found.

Discussion

While hearing loss is common in patients with XLH, pathophysiologic mechanisms of this hearing loss have been incompletely understood. To address this gap in medical knowledge, we combined functional hearing assessments with advanced histologic, histomorphometric, ultrastructural and mineralization analyses in *Hyp* mice. Our findings are consistent with the dominantly conductive hearing loss in *Hyp* mice because DPOAE thresholds shifts were larger than ABR threshold shifts, and DPOAE I/O function were rightward shifted in *Hyp* mice compared to WT mice. Specifically, sound energy passes through the middle ear twice for measurements of DPOAEs, and once for measurements of ABRs [30]. Consequently, there is a greater impact of conductive hearing loss on DPOAEs than on ABRs, with changes in DPOAE thresholds generally 1.5–2.5 times larger than in ABR thresholds at frequencies <30 kHz [30], as we observed. In addition, due to the linear sound processing of the middle ear, the DPOAE growth function remains unaltered in the presence of a sound conduction disturbance. This results in a DPOAE I/O function that is parallel to those in WT mice across different frequencies as observed in our study in *Hyp* mice. During cochlear perturbation, a steeper DPOAE I/O function would have been observed due to the non-linear sound processing of the inner ear [29].

Our subsequent in-depth analysis of the auditory ossicles to quantify their contribution to the observed conductive hearing loss in *Hyp* mice revealed severe hypomineralization (i.e., osteomalacia), which is typically observed at other skeletal sites in patients with XLH [6–10]. Interestingly and in contrast to WT mice during early development, which also exhibited voids in the ossicular bones, voids in *Hyp* mice represented cavities filled with unmineralized osteoid. These findings are consistent with the diffuse osteomalacia observed in *Hyp* mice [9,10,31] as well as in humans with XLH [32,33]. In WT mice, Matsuo was able to identify voids as large capillary loops lined with endothelial cells in the orbicular apophysis of the malleus during the first weeks of life [34]. In the close vicinity of these capillaries, specific type I and type II collagen-producing hypermineralizing “auditory osteoblasts” were

recently identified [35], and new matrix production led to a rapid decrease of the diameter of the capillaries [34]. Here, we were able to confirm this finding and demonstrated that matrix mineralization (i.e., CaMean) is further increased up to 24 weeks of age in WT mice, while the osteocyte lacunar number and area declined. These collective observations suggest that unmineralized areas in the ossicles of healthy young mice are regularly filled with mineral, whereas the newly formed bone (i.e., osteoid) in *Hyp* mice remains unmineralized, most likely representing a developmental phenomenon due to early hypophosphatemia.

The severity of altered bone mineralization of auditory ossicles might explain the conductive hearing loss we measured in *Hyp* mice. Ossicles are essential for normal hearing as they represent a dynamic, functional unit in the middle ear, transmitting the vibrations of the eardrum to the oval window, and hence fluids of the inner ear. Besides this role in sound transmission, the ossicles also influence the acoustic impedance matching and effectively amplify sound whose impedance is increased during transmission from air-filled middle ear to liquid-filled inner ear [36]. In humans, a high prevalence of hearing loss is also seen in patients with osteoporosis [37] and osteogenesis imperfecta [38,39]. Moreover, a significant correlation of BMD with conductive hearing capacity has been reported [40] underlining a potential role of bone quality (especially mineralization) in hearing conduction. In this context, it is interesting to note that the two included XLH patients with conductive hearing loss were also severely affected by skeletal symptoms, but larger clinical studies should investigate the possible relationship between disease severity, the degree of hypomineralization and conductive hearing loss.

In mice, there are a few other examples confirming the associations between bone remodeling abnormalities and hearing loss, one of them being the observation that bisphosphonates attenuated the bone loss in auditory ossicles and consequently ameliorated hearing loss [41]. It is also relevant that in FGF23-deficient mice, which also exhibit defective bone mineralization along with hyperphosphatemia and hypercalcemia [42], dysplastic changes of the ossicles, significant hearing loss with mixed conductive and sensorineural hearing loss were reported [43]. However, this study did not include the analysis of undecalcified sections, thus no conclusions regarding osteoid accumulation or matrix mineralization of the middle ear structures can be drawn.

Of note, analysis of the osteocyte lacunar characteristics revealed a significantly lowered total number of osteocyte lacunae in *Hyp* mice. A decreasing number of osteocyte lacunae along with tissue hypermineralization was previously demonstrated by our group in human ossicles with increasing age, indicative for early bone tissue aging [18]. Interestingly, we here also showed a declining number of osteocyte lacunae along with bone hypermineralization in the malleus of aging WT mice. Whether the reduction of osteocyte lacunar number in ossicles of *Hyp* mice along with severe hypomineralization is also caused by aging processes within the massive seams of osteoid remains to be elucidated. In addition to the anomalies in lacunar number, a significantly larger mean lacunar area was found in *Hyp* mice. An increase in osteocyte lacunar area has also been shown as a reversible phenomenon in vitamin D receptor (Vdr) deficient mice [44] as well as in lactating mice in the tibia and femur associated with increased demand of calcium from the skeletal calcium storage resulting in osteocyte-mediated perilacunar/canalicular bone remodeling [45]. An equivalent

mechanism of osteocytic osteolysis with enlarged osteocyte lacunae and the presence of markers such as cathepsin K and MMP-13 has also been demonstrated in the tibia and calvaria of *Hyp* mice [46]. Together, it is possible that the observed alterations in osteocyte lacunar properties indirectly affect hearing conduction *via* their effects on bone matrix quality.

Histologic analysis revealed in 5/7 *Hyp* mice ELHs in the basal turn of the cochlea, whereas WT mice showed no pathologic changes. Compared with the murine *Hyp-Duk* model [47,48], which presented severe ELHs in all specimens, mild ELHs, classified as grade 1 on the grading system of Melki et al. (2014) [23], were detected in *Hyp* mice. Considering these findings, *Hyp* mice can also be assumed to have a mild component of sensorineural hearing loss. Nevertheless, the conductive component seems to be the leading pathology. It has been shown that increased circulating FGF23, as in *Hyp* mice, causes volume expansion and hypertension by directly regulating Na^+-Cl^- cotransporter (NCC) in the distal renal tubules [49]. This FGF23 induced volume expansion is reversed by the NCC inhibitor chlorothiazide [49]. Chlorothiazide is an FDA-approved diuretic that has been used in Ménière's disease, a disorder associated with ELH that is characterized by recurrent episodes of fluctuating hearing loss, tinnitus, and vertigo. Inhibition of the NCC by chlorothiazide could therefore be considered as an option to treat ELH, but chlorothiazide does not cross the blood-brain-barrier under normal conditions and is therefore unlikely to cross the blood-labyrinth-barrier [50], which is why local application of chlorothiazide directly into the inner ear might be considered.

Burosumab, a human monoclonal antibody against FGF23 approved for the treatment of XLH, has been shown to increase renal phosphate reabsorption and thereby normalize serum phosphate levels, leading to reversibility of the mineralization defect as evidenced by recovery of osteoid indices [51]. In *Hyp* mice, similar effects of osteoid reduction were observed by vitamin D dietary supplementation [52]. Besides, treatment of *Hyp* mice with $1,25(OH)_2D$ or a FGF23 antibody showed reversibility of osteocytic osteolysis based on decreasing size of osteocyte lacunae and increasing canalicular connectivity [46]. It remains unanswered whether the mineralization defect of the ossicles along with detected conductive hearing loss is also reversible by specific treatments such as 25(OH)D, $1,25(OH)_2D$ or burosumab. As human ossicles are known not to significantly remodel after the first year of life [18], there may be a limited therapeutic window within which pharmacologic reversal of ossicular hypomineralization and hearing improvement may be possible. Defining that window should be pursued in future studies involving *Hyp* mice, with an eye toward rapid translation to clinic.

A limitation of our study is that we performed the auditory and skeletal analyses exclusively in male *Hyp* mice and their respective WT controls. However, despite the X-linked inheritance of the *PHEX* gene, no difference in disease severity of XLH between males and females could be found in previous studies [53,54]. Another limitation is that we performed the hearing tests and the detailed skeletal analyses in one age group only, and no therapeutic interventions could be implemented. Regardless of these limitations, this is the first study to investigate hearing and the micro-morphological osseous changes of the ossicles in *Hyp* mice.

In conclusion, we demonstrated conductive hearing loss associated with impaired ossicular mineralization in XLH patients and *Hyp* mice. Considering the relevance of auditory ossicles for mechanical sound conduction in the middle ear, this mineralization defect likely represents a major contributing factor to conductive hearing loss in XLH. As hearing loss represents a relevant comorbidity in XLH, routine evaluation of hearing should be performed in XLH patients, with accurate differentiation between conductive and sensorineural components. The effect of therapeutic agents that attenuate osteomalacia like 25(OH)D, $1,25(OH)_2D$ or the FGF23 antibody burosumab on the hearing function and ossicular mineralization should be elucidated in future studies. Based on our findings, early treatment of XLH may be crucial to preserve the mineralization of auditory ossicles.

Supplementary Material

Refer to Web version on PubMed Central for supplementary material.

Acknowledgments:

We thank Olga Winter, Andrea Thieke and Elke Leicht for technical assistance with the histological sections.

Funding: These studies were supported by grants from the German Research Foundation (RO 5925/1-1 to TR) and the National Institutes of Health (R01-AR072650-01 to MBD). KMS acknowledges support of the National Institutes of Health grant R01-DC015824, Nancy Sayles Day Foundation, the Barnes Foundation, and Sheldon and Dorothea Buckler. Parts of the presented human data were generated within the BLIX Study (Bone quaLity In XLH) funded by Kyowa Kirin International to RO.

References

1. Beck-Nielsen SS, Brock-Jacobsen B, Gram J, Brixen K, Jensen TK. Incidence and prevalence of nutritional and hereditary rickets in southern Denmark. Eur J Endocrinol. 2009;160(3):491–7. [PubMed: 19095780]
2. Liu S, Guo R, Simpson LG, Xiao ZS, Burnham CE, Quarles LD. Regulation of fibroblastic growth factor 23 expression but not degradation by PHEX. J Biol Chem. 2003;278(39):37419–26. [PubMed: 12874285]
3. Murali SK, Andrukhova O, Clinkenbeard EL, White KE, Erben RG. Excessive Osteocytic Fgf23 Secretion Contributes to Pyrophosphate Accumulation and Mineralization Defect in Hyp Mice. PLoS Biol. 2016;14(4):e1002427. [PubMed: 27035636]
4. Haffner D, Emma F, Eastwood DM, Duplan MB, Bacchetta J, Schnabel D, et al. Clinical practice recommendations for the diagnosis and management of X-linked hypophosphataemia. Nat Rev Nephrol. 2019;15(7):435–55. [PubMed: 31068690]
5. Lane NE, Parimi N, Corr M, Yao W, Cauley JA, Nielson CM, et al. Association of serum fibroblast growth factor 23 (FGF23) and incident fractures in older men: the Osteoporotic Fractures in Men (MrOS) study. J Bone Miner Res. 2013;28(11):2325–32. [PubMed: 23677793]
6. Shanbhogue VV, Hansen S, Folkestad L, Brixen K, Beck-Nielsen SS. Bone geometry, volumetric density, microarchitecture, and estimated bone strength assessed by HR-pQCT in adult patients with hypophosphatemic rickets. J Bone Miner Res. 2015;30(1):176–83. [PubMed: 25042721]
7. Murali SK, Roschger P, Zeitz U, Klaushofer K, Andrukhova O, Erben RG. FGF23 Regulates Bone Mineralization in a 1,25(OH)2 D3 and Klotho-Independent Manner. J Bone Miner Res. 2016;31(1):129–42. [PubMed: 26235988]
8. Fratzl-Zelman N, Gamsjaeger S, Blouin S, Kocijan R, Plasenzotti P, Rokidi S, et al. Alterations of bone material properties in adult patients with X-linked hypophosphatemia (XLH). J Struct Biol. 2020;211(3):107556. [PubMed: 32619592]

9. Brownstein CA, Zhang J, Stillman A, Ellis B, Troiano N, Adams DJ, et al. Increased bone volume and correction of HYP mouse hypophosphatemia in the Klotho/HYP mouse. Endocrinology. 2010;151(2):492–501. [PubMed: 19952276]
10. Liu ES, Martins JS, Raimann A, Chae BT, Brooks DJ, Jorgetti V, et al. 1,25-Dihydroxyvitamin D Alone Improves Skeletal Growth, Microarchitecture, and Strength in a Murine Model of XLH, Despite Enhanced FGF23 Expression. J Bone Miner Res. 2016;31(5):929–39. [PubMed: 26751835]
11. Carpenter TO, Imel EA, Holm IA, Jan de Beur SM, Insogna KL. A clinician's guide to X-linked hypophosphatemia. J Bone Miner Res. 2011;26(7):1381–8. [PubMed: 21538511]
12. Chanchlani R, Nemer P, Sinha R, Nemer L, Krishnappa V, Sochett E, et al. An Overview of Rickets in Children. Kidney Int Rep. 2020;5(7):980–90. [PubMed: 32647755]
13. Rothenbuhler A, Fadel N, Debza Y, Bacchetta J, Diallo MT, Adamsbaum C, et al. High Incidence of Cranial Synostosis and Chiari I Malformation in Children With X-Linked Hypophosphatemic Rickets (XLHR). J Bone Miner Res. 2019;34(3):490–6. [PubMed: 30352126]
14. Chesher D, Oddy M, Darbar U, Sayal P, Casey A, Ryan A, et al. Outcome of adult patients with X-linked hypophosphatemia caused by PHEX gene mutations. J Inherit Metab Dis. 2018;41(5):865–76. [PubMed: 29460029]
15. Beck-Nielsen SS, Mughal Z, Haffner D, Nilsson O, Levtchenko E, Ariceta G, et al. FGF23 and its role in X-linked hypophosphatemia-related morbidity. Orphanet J Rare Dis. 2019;14(1):58. [PubMed: 30808384]
16. Davies M, Kane R, Valentine J. Impaired hearing in X-linked hypophosphataemic (vitamin-D-resistant) osteomalacia. Ann Intern Med. 1984;100(2):230–2. [PubMed: 6691666]
17. Ivanovic-Zuvic D, Santander MJ, Jimenez M, Novoa I, Winter M, Florenzano P. Characterization of otologic involvement in patients with X-Linked Hypophosphatemia. Clin Otolaryngol. 2021.
18. Rolvien T, Schmidt FN, Milovanovic P, Jahn K, Riedel C, Butscheidt S, et al. Early bone tissue aging in human auditory ossicles is accompanied by excessive hypermineralization, osteocyte death and micropetrosis. Sci Rep. 2018;8(1):1920. [PubMed: 29382878]
19. Schmidt FN, Delsmann MM, Mletzko K, Yorgan TA, Hahn M, Siebert U, et al. Ultra-high matrix mineralization of sperm whale auditory ossicles facilitates high sound pressure and high-frequency underwater hearing. Proc Biol Sci. 2018;285:20181820. [PubMed: 30963901]
20. Priemel M, von Domarus C, Klatte TO, Kessler S, Schlie J, Meier S, et al. Bone mineralization defects and vitamin D deficiency: histomorphometric analysis of iliac crest bone biopsies and circulating 25-hydroxyvitamin D in 675 patients. J Bone Miner Res. 2010;25(2):305–12. [PubMed: 19594303]
21. Ison JR, Allen PD, O'Neill WE. Age-related hearing loss in C57BL/6J mice has both frequency-specific and non-frequency-specific components that produce a hyperacusis-like exaggeration of the acoustic startle reflex. J Assoc Res Otolaryngol. 2007;8(4):539–50. [PubMed: 17952509]
22. Schmidt PH, Eggermont JJ, Odenthal DW. Study of meniere's disease by electrocochleography. Acta Otolaryngol Suppl. 1974;316:75–84. [PubMed: 4525923]
23. Melki SJ, Li Y, Semaan MT, Zheng QY, Megerian CA, Alagramam KN. A mouse model validates the utility of electrocochleography in verifying endolymphatic hydrops. J Assoc Res Otolaryngol. 2014;15(3):413–21. [PubMed: 24509791]
24. Dempster DW, Compston JE, Drezner MK, Glorieux FH, Kanis JA, Malluche H, et al. Standardized nomenclature, symbols, and units for bone histomorphometry: a 2012 update of the report of the ASBMR Histomorphometry Nomenclature Committee. J Bone Miner Res. 2013;28(1):2–17. [PubMed: 23197339]
25. Busse B, Djonic D, Milovanovic P, Hahn M, Puschel K, Ritchie RO, et al. Decrease in the osteocyte lacunar density accompanied by hypermineralized lacunar occlusion reveals failure and delay of remodeling in aged human bone. Aging Cell. 2010;9(6):1065–75. [PubMed: 20874757]
26. Roschger P, Paschalis EP, Fratzl P, Klaushofer K. Bone mineralization density distribution in health and disease. Bone. 2008;42(3):456–66. [PubMed: 18096457]
27. Zimmermann EA, Riedel C, Schmidt FN, Stockhausen KE, Chushkin Y, Schaible E, et al. Mechanical Competence and Bone Quality Develop During Skeletal Growth. J Bone Miner Res. 2019;34(8):1461–72. [PubMed: 30913317]

28. Roschger P, Plenk H Jr., Klaushofer K, Eschberger J. A new scanning electron microscopy approach to the quantification of bone mineral distribution: backscattered electron image grey-levels correlated to calcium K alpha-line intensities. Scanning Microsc. 1995;9(1):75–86; discussion −8. [PubMed: 8553027]
29. Gehr DD, Janssen T, Michaelis CE, Deingruber K, Lamm K. Middle ear and cochlear disorders result in different DPOAE growth behaviour: implications for the differentiation of sound conductive and cochlear hearing loss. Hear Res. 2004;193(1–2):9–19. [PubMed: 15219315]
30. Qin Z, Wood M, Rosowski JJ. Measurement of conductive hearing loss in mice. Hear Res. 2010;263(1–2):93–103. [PubMed: 19835942]
31. Yuan B, Takaiwa M, Clemens TL, Feng JQ, Kumar R, Rowe PS, et al. Aberrant Phex function in osteoblasts and osteocytes alone underlies murine X-linked hypophosphatemia. J Clin Invest. 2008;118(2):722–34. [PubMed: 18172553]
32. Dahir K, Roberts MS, Krolczyk S, Simmons JH. X-Linked Hypophosphatemia: A New Era in Management. J Endocr Soc. 2020;4(12):bvaa151. [PubMed: 33204932]
33. Robinson ME, AlQuorain H, Murshed M, Rauch F. Mineralized tissues in hypophosphatemic rickets. Pediatr Nephrol. 2020;35(10):1843–54. [PubMed: 31392510]
34. Matsuo K, Kuroda Y, Nango N, Shimoda K, Kubota Y, Ema M, et al. Osteogenic capillaries orchestrate growth plate-independent ossification of the malleus. Development. 2015;142(22):3912–20. [PubMed: 26428006]
35. Kuroda Y, Kawaai K, Hatano N, Wu Y, Takano H, Momose A, et al. Hypermineralization of Hearing-Related Bones by a Specific Osteoblast Subtype. J Bone Miner Res. 2021;36(8):1535–47. [PubMed: 33905562]
36. Kurokawa H, Goode RL. Sound pressure gain produced by the human middle ear. Otolaryngol Head Neck Surg. 1995;113(4):349–55. [PubMed: 7567003]
37. Upala S, Rattanawong P, Vutthikraivit W, Sanguankeo A. Significant association between osteoporosis and hearing loss: a systematic review and meta-analysis. Braz J Otorhinolaryngol. 2017;83(6):646–52. [PubMed: 27670202]
38. Pillion JP, Vernick D, Shapiro J. Hearing loss in osteogenesis imperfecta: characteristics and treatment considerations. Genet Res Int. 2011;2011:983942. [PubMed: 22567374]
39. Ma X, Wang F, Shen W, Yang S. The impact of stapes surgery on osteogenesis imperfecta: a retrospective comparison of operative outcomes with those for patients with otosclerosis. Acta Otolaryngol. 2020;140(11):930–8. [PubMed: 32692268]
40. Ozkiris M, Karacavus S, Kapusuz Z, Balbaloglu O, Saydam L. Does bone mineral density have an effect on hearing loss in postmenopausal patients? Ann Otol Rhinol Laryngol. 2013;122(10):648–52. [PubMed: 24294688]
41. Kanzaki S, Takada Y, Ogawa K, Matsuo K. Bisphosphonate therapy ameliorates hearing loss in mice lacking osteoprotegerin. J Bone Miner Res. 2009;24(1):43–9. [PubMed: 18715136]
42. Shimada T, Kakitani M, Yamazaki Y, Hasegawa H, Takeuchi Y, Fujita T, et al. Targeted ablation of Fgf23 demonstrates an essential physiological role of FGF23 in phosphate and vitamin D metabolism. J Clin Invest. 2004;113(4):561–8. [PubMed: 14966565]
43. Lysaght AC, Yuan Q, Fan Y, Kalwani N, Caruso P, Cunnane M, et al. FGF23 deficiency leads to mixed hearing loss and middle ear malformation in mice. PLoS One. 2014;9(9):e107681. [PubMed: 25243481]
44. Rolvien T, Krause M, Jeschke A, Yorgan T, Puschel K, Schinke T, et al. Vitamin D regulates osteocyte survival and perilacunar remodeling in human and murine bone. Bone. 2017;103:78–87. [PubMed: 28666969]
45. Qing H, Ardeshirpour L, Pajevic PD, Dusevich V, Jahn K, Kato S, et al. Demonstration of osteocytic perilacunar/canalicular remodeling in mice during lactation. J Bone Miner Res. 2012;27(5):1018–29. [PubMed: 22308018]
46. Tokarz D, Martins JS, Petit ET, Lin CP, Demay MB, Liu ES. Hormonal Regulation of Osteocyte Perilacunar and Canalicular Remodeling in the Hyp Mouse Model of X-Linked Hypophosphatemia. J Bone Miner Res. 2018;33(3):499–509. [PubMed: 29083055]

47. Wick CC, Lin SJ, Yu H, Megerian CA, Zheng QY. Treatment of ear and bone disease in the Phex mouse mutant with dietary supplementation. Am J Otolaryngol. 2017;38(1):44–51. [PubMed: 27733274]

48. Megerian CA, Semaan MT, Aftab S, Kisley LB, Zheng QY, Pawlowski KS, et al. A mouse model with postnatal endolymphatic hydrops and hearing loss. Hear Res. 2008;237(1–2):90–105. [PubMed: 18289812]

49. Andrukhova O, Slavic S, Smorodchenko A, Zeitz U, Shalhoub V, Lanske B, et al. FGF23 regulates renal sodium handling and blood pressure. EMBO Mol Med. 2014;6(6):744–59. [PubMed: 24797667]

50. Sigaroudi A, Kinzig M, Wahl O, Stelzer C, Schroeter M, Fuhr U, et al. Quantification of Hydrochlorothiazide and Ramipril/Ramiprilate in Blood Serum and Cerebrospinal Fluid: A Pharmacokinetic Assessment of Central Nervous System Adverse Effects. Pharmacology. 2018;102(3–4):133–7. [PubMed: 29982257]

51. Insogna KL, Rauch F, Kamenicky P, Ito N, Kubota T, Nakamura A, et al. Burosumab Improved Histomorphometric Measures of Osteomalacia in Adults with X-Linked Hypophosphatemia: A Phase 3, Single-Arm, International Trial. J Bone Miner Res. 2019;34(12):2183–91. [PubMed: 31369697]

52. Barratt KR, Sawyer RK, Atkins GJ, St-Arnaud R, Anderson PH. Vitamin D supplementation improves bone mineralisation independent of dietary phosphate in male X-linked hypophosphatemic (Hyp) mice. Bone. 2021;143:115767. [PubMed: 33232838]

53. Zhang C, Zhao Z, Sun Y, Xu L, JiaJue R, Cui L, et al. Clinical and genetic analysis in a large Chinese cohort of patients with X-linked hypophosphatemia. Bone. 2019;121:212–20. [PubMed: 30682568]

54. Whyte MP, Schranck FW, Armamento-Villareal R. X-linked hypophosphatemia: a search for gender, race, anticipation, or parent of origin effects on disease expression in children. J Clin Endocrinol Metab. 1996;81(11):4075–80. [PubMed: 8923863]

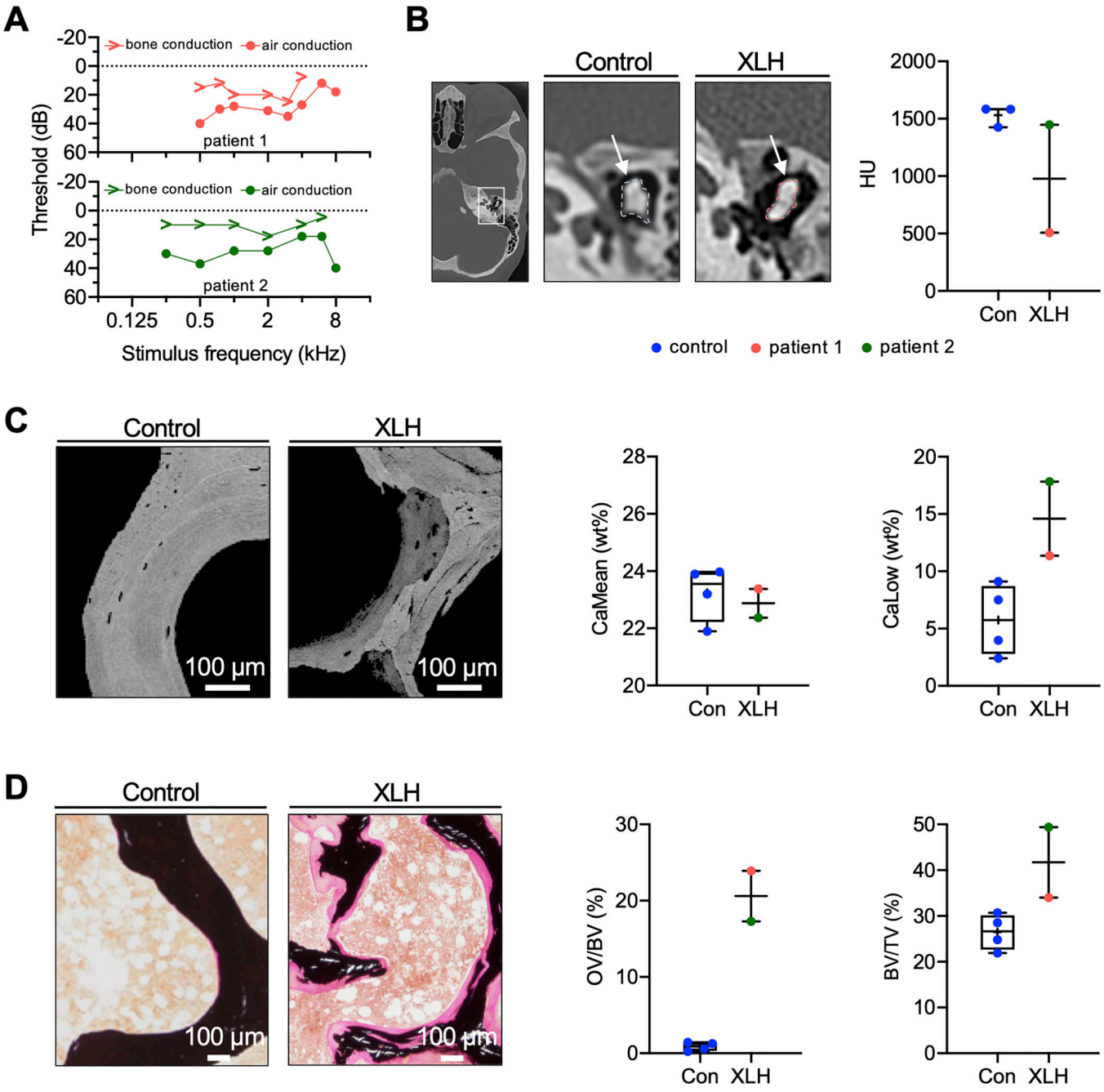

Fig. 1. Conductive hearing loss and severe osteomalacia in patients with XLH.

(A) Pure-tone threshold audiometry of a 27-year-old (patient 1) and a 32-year-old (patient 2) woman with XLH. While both sides were equally affected, the representative measurements of the right ears are shown. The sound frequency (in kHz) is shown on the horizontal axis of the audiogram, while the sound intensity (in dB) is recorded on the vertical axis. The thresholds of bone and air conduction are displayed as arrowheads and circles, respectively. Results revealed higher air conduction thresholds indicating conductive hearing loss. (B) Left: CCT images showing representative auditory ossicles of a control and XLH patient. White arrows point to the measured region of interest. Right: Quantification of average

hounsfield units (HU) in two XLH patients and controls. (C) Representative qBEI images of a transiliac crest biopsy of the XLH patients and of healthy age-matched controls. Bone mineral density distribution analysis showed reduced CaMean and increased fraction of CaLow in XLH. (D) Representative von Kossa-van Gieson stained histological images, showing increased OV/BV and BV/TV of the XLH patient compared to age-matched controls.

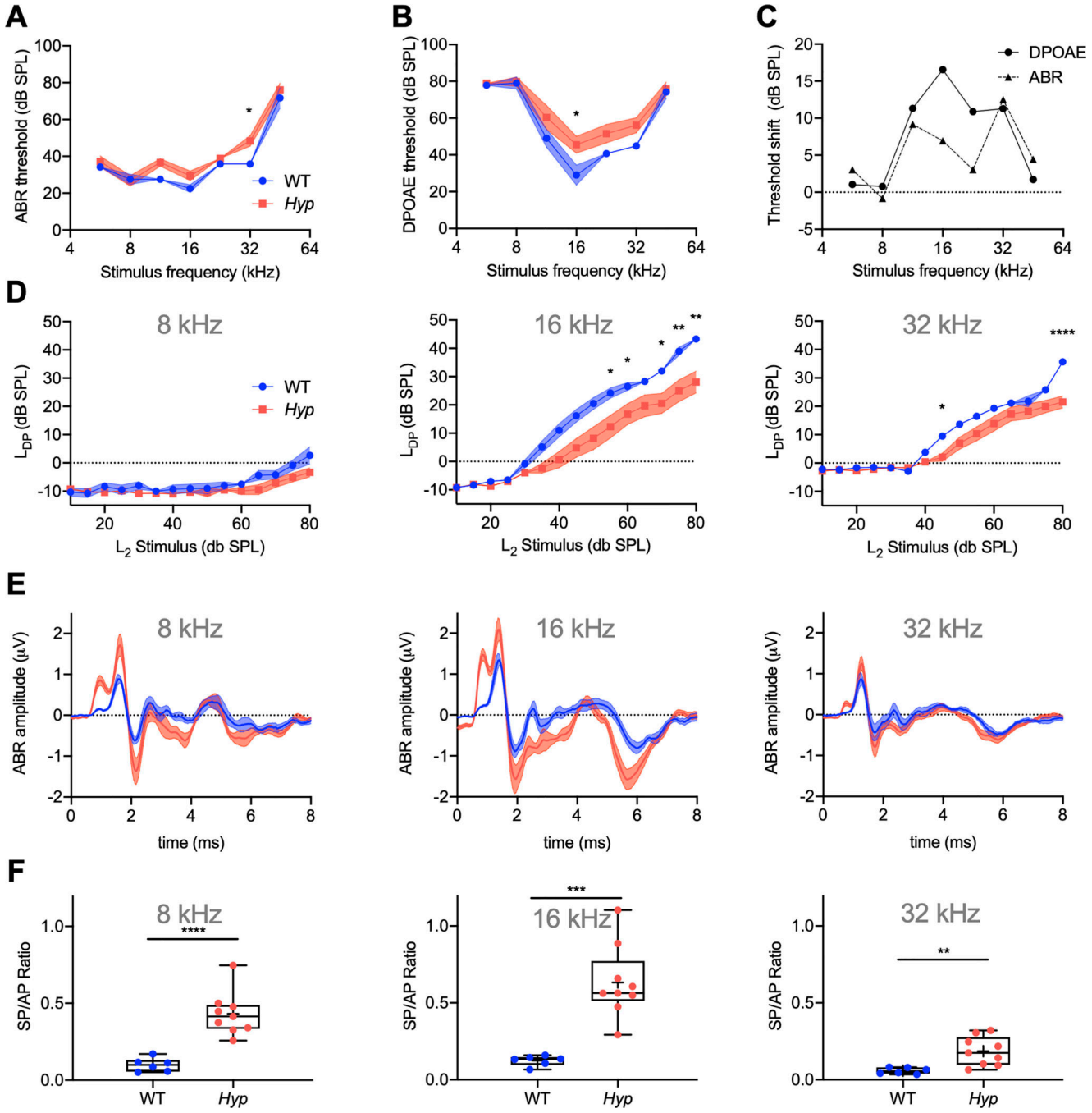

Fig. 2. Hyp mice exhibit increased ABR and DPOAE thresholds, shifts in DPOAE I/O functions consistent with conductive hearing loss.

(A) ABR and (B) DPOAEs were measured in 6-week-old male WT (blue curve) and *Hyp* (red curve) mice from mixed litters. (C) Threshold shifts between WT and *Hyp* mice were similar in ABRs and DPOAEs, except for the mid-frequency region spanning 16.0 – 22.65 kHz where DPOAE shifts (solid line) were about twice as large as ABR shifts (dashed line). (D) DPOAE I/O-functions at 8, 16 and 32 kHz. (E, F) SP/AP ratios at 8, 16 and 32 kHz are increased in *Hyp* mice (red curve/column) compared to WT mice (blue curve/

column). *p<0.05, **p< 0.01, ***p<0.001, ****p<0.0001 (2-way ANOVA with Sidak's test for multiple comparisons and two-tailed unpaired *t*-test).

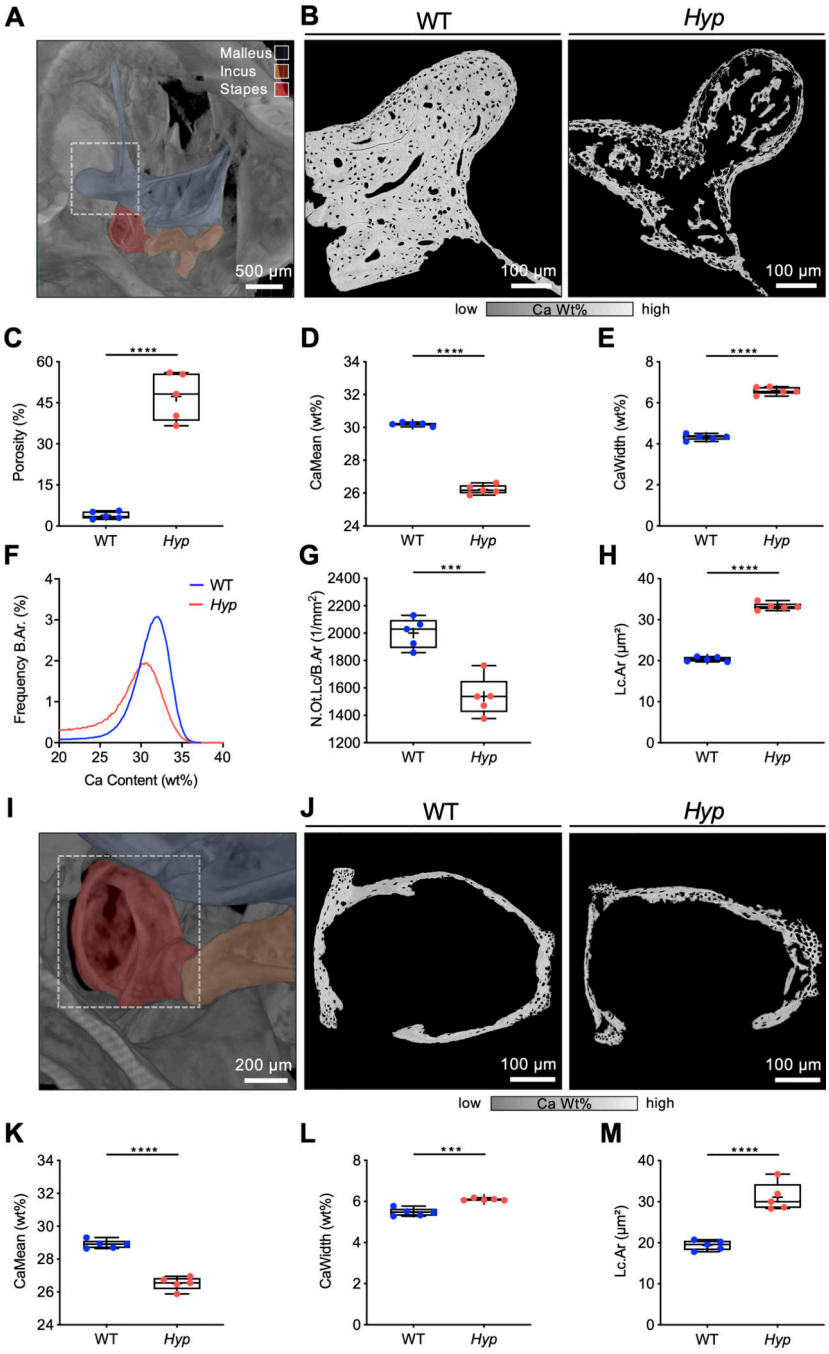

Fig. 3. Irregular and reduced mineralization of the malleus and stapes evaluated by qBEI in WT and *Hyp* mice.

(A) A representative three-dimensional reconstruction of µCT-imaging of a murine WT middle ear (24-week-old male mice) with virtual fenestration of the temporal bone and pseudocolors highlighting the anatomical localization of the ossicles. (B-H) qBEI analysis of the malleus. (B) Representative qBEI images of the malleus of WT (left panel) and *Hyp* mice (right panel). (C) Analysis of the porosity, (D) mean calcium content (CaMean) and (E) width of the distribution of mineralization levels (CaWidth) in WT and *Hyp* mice. (F) Bone mineral density distribution (BMDD) histograms of the mineralization of the

mallei of WT (blue curve) and *Hyp* mice (red curve). (G, H) Quantification of the number (N.Ot.Lc/B.Ar) and mean area of osteocyte lacunae (Lc.Ar) in *Hyp* mice compared to WT. (I) µCT-image of the middle ear with focus on the stapes marked in red. (J) Representative qBEI images of the stapes in WT (left panel) and *Hyp* mice (right panel). (K) Quantification of the mean calcium content (CaMean) in *Hyp* mice compared to WT, (L) mineralization heterogeneity (CaWidth) and (M) the mean osteocyte lacunar area (Lc.Ar). ***p<0.001, ****p<0.0001 (two-tailed unpaired *t*-test).

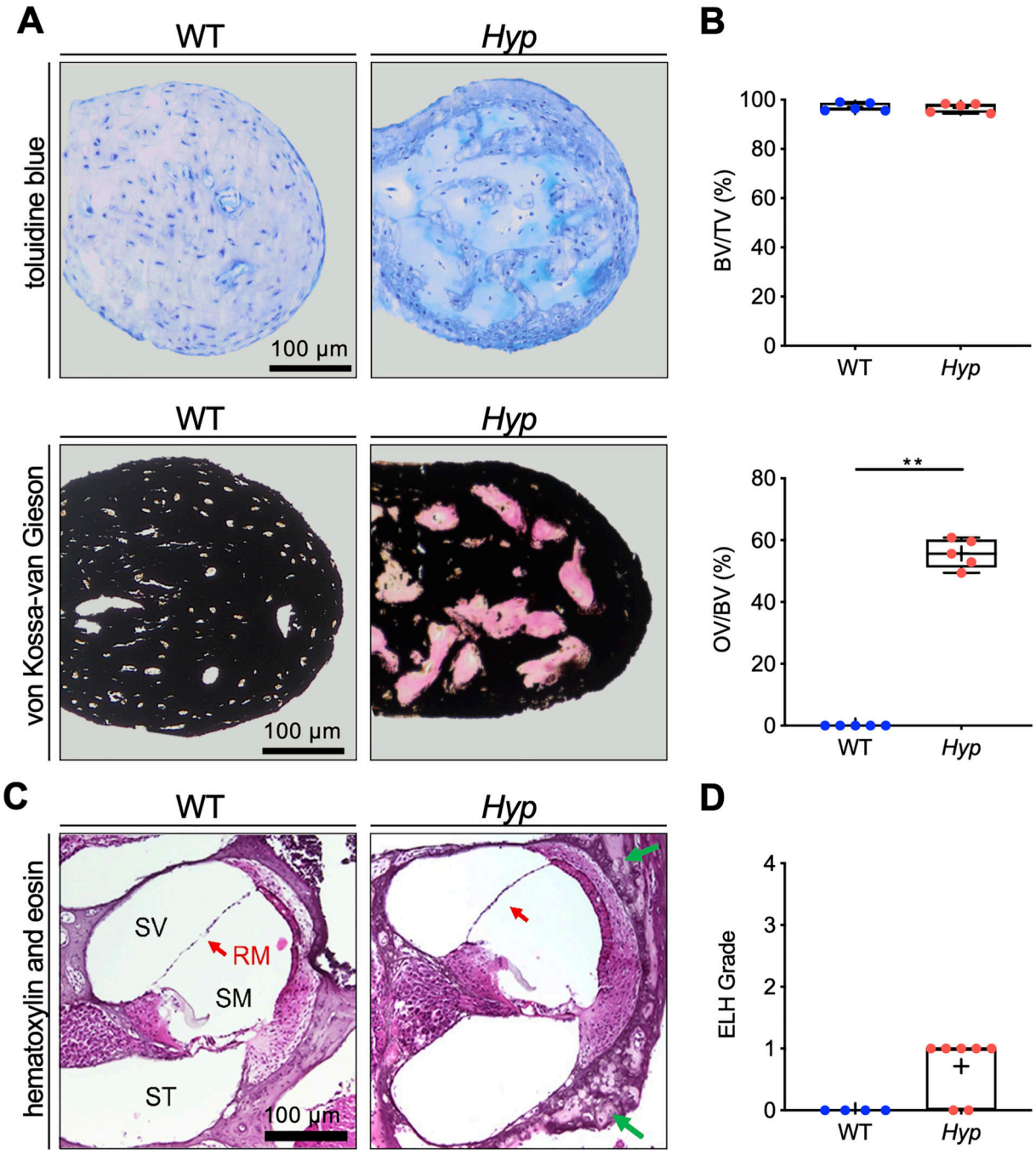

Fig. 4. Undecalcified histology identifies osteoid accumulation in the malleus and signs of mild endolymphatic hydrops in the cochlea in *Hyp* mice.

(A) Representative histological images of toluidine blue stained orbicular apophysis of the malleus of 24-week-old *Hyp* and WT mice (upper panel) and von Kossa-van Gieson staining (lower panel). (B) Evaluation of bone volume fraction (BV/TV; upper panel), osteoid volume per bone volume (OV/BV; lower panel) in *Hyp* mice compared to WT. (C) Representative cochlear cross-sections from 6-week-old male WT (left panel) and *Hyp* mice (right panel) in hematoxylin and eosin (H&E) staining. The otic capsule in *Hyp* mice shows osteoidosis (green arrows) and a bulging Reissner's membrane (RM, red arrow). (D)

Endolymphatic hydrops (ELH) in the basal turn classified into the severity grades [23]. ELH was not observed in WT animals whereas grade 1 ELH was detected in five out of seven analyzed *Hyp* animals. **p<0.01 (two-tailed unpaired *t*-test and Mann-Whitney-U-test).

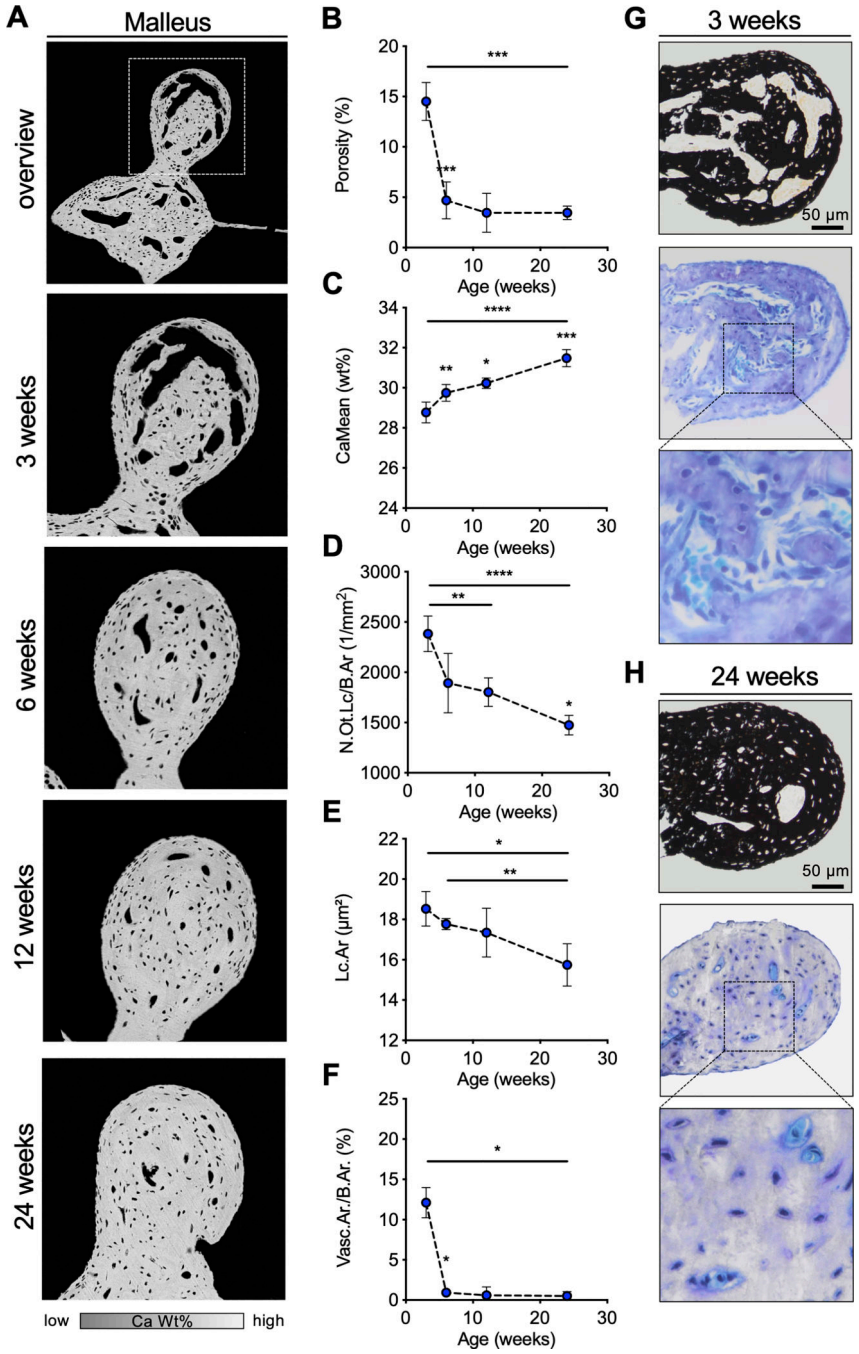

Fig. 5. Postnatal development of the ossicles in WT mice.

(A) qBEI images of the orbicular apophysis of the malleus at selected timepoints. (B, C) Quantification of the osseous porosity, CaMean and CaPeak. (D, E) Analysis of the number of osteocyte lacunae per bone (N.Ot.Lc/B.Ar) and the mean osteocyte lacunar area (Lc.Ar). (F) Quantification of the vascular area per bone area (Vasc.Ar/B.Ar). (G, H) Histological images (von Kossa-van Gieson and toluidine blue staining) of the malleus at the age of 3

weeks and 24 weeks indicating the reduction of porosity with age in WT mice. *p<0.05, **p<0.01, ***p<0.001, ****p<0.0001 (two-tailed paired *t*-test).